INTERNATIONAL JOURNAL FOR NUMERICAL METHODS IN FLUIDS
Int. J. Numer. Meth. Fluids 2002; **38**:139–161 (DOI: 10.1002/fld.206)

High-resolution, monotone solution of the adjoint shallow-water equations

Brett F. Sanders[1,†] and Scott F. Bradford[2]

[1]*Department of Civil and Environmental Engineering, University of California, Irvine, CA 92697, U.S.A.*
[2]*Naval Research Laboratory, Washington DC, 20375, U.S.A.*

SUMMARY

A monotone, second-order accurate numerical scheme is presented for solving the differential form of the adjoint shallow-water equations in generalized two-dimensional coordinates. Fluctuation-splitting is utilized to achieve a high-resolution solution of the equations in primitive form. One-step and two-step schemes are presented and shown to achieve solutions of similarly high accuracy in one dimension. However, the two-step method is shown to yield more accurate solutions to problems in which unsteady wave speeds are present. In two dimensions, the two-step scheme is tested in the context of two parameter identification problems, and it is shown to accurately transmit the information needed to identify unknown forcing parameters based on measurements of the system response. The first problem involves the identification of an upstream flood hydrograph based on downstream depth measurements. The second problem involves the identification of a long wave state in the far-field based on near-field depth measurements. Copyright © 2002 John Wiley & Sons, Ltd.

KEY WORDS: shallow-water model; adjoint equation method; parameter identification; finite volume method

INTRODUCTION

Adjoint equation methods are efficient techniques for evaluating the response of mathematically modeled systems to perturbations in state variables or model parameters [1]. The solution to a single adjoint equation or system of equations determines the dependence of a functional of the model solution to independent perturbations of model variables at any time or location. Using a system measurement, the adjoint equation solution permits identification of model parameters [2–6] and initial or boundary conditions [7–10] that created the system response. In either case, a system of adjoint equations must be solved that is similar in form to the original system of equations representing conservation of mass, momentum, and possibly energy. The latter equations are termed the *direct problem*, while the prior are termed the *adjoint problem*.

*Correspondence to: B. F. Sanders, Department of Civil and Environmental Engineering, University of California, Irvine, CA 92697, U.S.A.
† E-mail: bsanders@uci.edu

Received July 1999
Revised March 2001

It is possible to derive the adjoint equations in either a discrete form from the discretized equations of the direct problem, or to derive them in a differential form from the continuous conservation equations. In the latter case, the differential form of the adjoint equations must subsequently be discretized and solved, which is the approach adopted in this study.

The finite volume method is well known for the solution of the Euler equations describing compressible gas dynamics, and has more recently been applied for the solution of the shallow-water equations [11–14] and for the solution of the depth integrated equations describing turbidity current hydrodynamics [15]. The method is ideal for solving hyperbolic conservation laws that admit discontinuous solutions, because it accurately captures waves and flow discontinuities are sharply resolved but free of spurious oscillations [16]. Therefore, a finite volume method is used in this study to solve the direct problem.

The monotonicity-preserving and high-resolution properties of the finite volume method also make it attractive for solving the adjoint problem. However, the method is attractive for several additional reasons. First, non-reflecting boundary conditions are easily implemented. It has been shown that non-reflecting boundaries should be implemented in the adjoint problem when evaluating sensitivities for water wave control problems [17]. Second, characteristic variables of the adjoint problem are accurately computed. Characteristic variables contain information on the response of the modeled system to perturbations in the flow [17], and the Riemann solvers inherent to Godunov-type finite volume schemes yield accurate estimates of the characteristic variables. Third, the adjoint problem is driven by a point source within the solution domain, as opposed to boundary and initial conditions as is the case of the shallow-water equations. This source has been found to cause instabilities in finite-difference schemes [18], but are easily handled in a finite volume-type algorithm. Hence, an accurate, stable, and monotone solution of the adjoint equations is possible with the finite volume method. While the performance of adjoint methods in the presence of direct problem discontinuities is poorly understood, the finite volume method permits a stable adjoint problem solution in the presence of either direct problem or adjoint problem discontinuities.

Unfortunately, the finite volume method is designed for the discretization of conservation laws, which the adjoint shallow-water equations are not. In the present study, the fluctuation splitting technique developed by Roe [19] is the basis of a finite volume method to solve the adjoint equations in primitive form. Two alternative finite volume fluctuation-splitting approaches are presented in this paper. The first is a one-step approach most recently presented by LeVeque [20], while the second is a predictor-corrector approach in the spirit of Hancock's method, which was first applied to solve the Euler equations [21]. In the following sections, the shallow-water and adjoint shallow-water equations are presented, two alternative approaches to solve the adjoint shallow-water equations are presented, and a series of numerical tests to examine the performance of the proposed schemes is presented and the results are discussed.

THE SHALLOW-WATER EQUATIONS

The shallow-water equations are a system of quasi-linear hyperbolic conservation laws and therefore can be written in integral form as

$$\frac{\partial}{\partial t}\int_{\Omega}\mathbf{U}\,\mathrm{d}\Omega+\oint_{\partial\Omega}(\mathbf{F}\,\mathrm{d}y-\mathbf{G}\,\mathrm{d}x)=\int_{\Omega}\mathbf{S}\,\mathrm{d}\Omega \tag{1}$$

where Ω represents a spatial domain and $\mathbf{U}^T = (h\ hu\ hv)$. The fluxes and source terms are defined as

$$\mathbf{F} = \begin{pmatrix} uh \\ u^2h + \dfrac{gh^2}{2} \\ uvh \end{pmatrix} \quad \mathbf{G} = \begin{pmatrix} vh \\ uvh \\ v^2h + \dfrac{gh^2}{2} \end{pmatrix} \quad \mathbf{S} = \begin{pmatrix} 0 \\ gh(S_{ox} - S_{fx}) \\ gh(S_{oy} - S_{fy}) \end{pmatrix}$$

where h is the flow depth, u and v are the depth averaged flow velocities in the x and y directions, respectively, and the terms in $\mathbf{S}$ represent the bed and friction slopes and are given as,

$$S_{ox} = -\frac{\partial z}{\partial x} \qquad S_{oy} = -\frac{\partial z}{\partial y} \tag{2}$$

and

$$S_{fx} = \frac{n^2 u\sqrt{u^2 + v^2}}{h^{4/3}} \qquad S_{fy} = \frac{n^2 v\sqrt{u^2 + v^2}}{h^{4/3}} \tag{3}$$

where $z = z(x, y)$ is the bed elevation above an arbitrary datum and n is the Manning coefficient of bed resistance.

THE ADJOINT SHALLOW-WATER EQUATIONS

The adjoint shallow-water equations are derived by formulating a Lagrangian, which is the sum of an objective function and physical constraints multiplied by Lagrange or adjoint variables. The objective function may be defined as,

$$J = \int_0^T \int_\Omega r(h(x, y, t), p(x, y, t), q(x, y, t))\, \mathrm{d}\Omega\, \mathrm{d}t \tag{4}$$

where r is a measuring function, $p = uh$, and $q = vh$. The physical constraints consist of the mass and momentum conservation laws, i.e. Equation (1). Green's theorem may be used to convert the boundary integral to an area integral, provided that $\mathbf{F}$ and $\mathbf{G}$ are continuous. The Lagrangian is then defined as,

$$\begin{aligned} \mathscr{L} = J &+ \int_0^T \int_\Omega \phi \left[\frac{\partial h}{\partial t} + \frac{\partial p}{\partial x} + \frac{\partial q}{\partial y} \right] \\ &+ \psi_x \left[\frac{\partial p}{\partial t} + \frac{\partial}{\partial x}\left(\frac{p^2}{h} + \frac{gh^2}{2} \right) + \frac{\partial}{\partial y}\left(\frac{pq}{h} \right) - gh(S_{ox} - S_{fx}) \right] \\ &+ \psi_y \left[\frac{\partial q}{\partial t} + \frac{\partial}{\partial x}\left(\frac{pq}{h} \right) + \frac{\partial}{\partial y}\left(\frac{q^2}{h} + \frac{gh^2}{2} \right) - gh(S_{oy} - S_{fy}) \right] \mathrm{d}\Omega\, \mathrm{d}t = 0 \end{aligned} \tag{5}$$

The adjoint shallow-water equations follow from setting the partial derivatives of the Lagrangian with respect to h, p, and q to zero and are given as [17],

$$\frac{\partial \mathbf{\Phi}}{\partial \tau} + \mathbf{A}_\Phi \frac{\partial \mathbf{\Phi}}{\partial x} + \mathbf{B}_\Phi \frac{\partial \mathbf{\Phi}}{\partial y} + \mathbf{C}_\Phi \mathbf{\Phi} + \mathbf{D}_\Phi = 0 \tag{6}$$

where $\tau = T - t$ is the inverse time direction, $\mathbf{\Phi} = (\phi \ \psi_x \ \psi_y)^T$, $\mathbf{D}_\Phi = (\partial r/\partial h \ \ \partial r/\partial p \ \ \partial r/\partial q)^T$ and

$$\mathbf{A}_\Phi = \begin{pmatrix} 0 & u^2 - a^2 & uv \\ -1 & -2u & -v \\ 0 & 0 & -u \end{pmatrix} \quad \mathbf{B}_\Phi = \begin{pmatrix} 0 & uv & v^2 - a^2 \\ 0 & -v & 0 \\ -1 & -u & -2v \end{pmatrix} \tag{7}$$

$$\mathbf{C}_\Phi = \begin{pmatrix} 0 & -g(S_{ox} + \frac{7}{3}S_{fx}) & -g(S_{oy} + \frac{7}{3}S_{fy}) \\ 0 & -g\dfrac{2u^2 + v^2}{u(u^2 + v^2)}S_{fx} & -g\dfrac{u}{u^2 + v^2}S_{fy} \\ 0 & -g\dfrac{v}{u^2 + v^2}S_{fx} & -g\dfrac{u^2 + 2v^2}{v(u^2 + v^2)}S_{fy} \end{pmatrix} \tag{8}$$

and $a = (gh)^{1/2}$ is the speed of an elementary gravity wave.

As is indicated by the form of Equation (6), the adjoint equations naturally appear in non-conservation form. The shallow-water equations have both a non-conservative and a conservative form, so one might expect the adjoint shallow-water equations to also have a conservation form. However, this is not the case. No similarity transformation of the adjoint shallow-water equations is possible. This is not surprising since the adjoint shallow-water equations are not derived as conservation laws, but are instead the result of manipulating conservation laws.

NUMERICAL SOLUTION OF THE SHALLOW WATER EQUATIONS

A finite volume scheme known as Hancock's method is utilized here to solve the shallow-water equations [21]. This scheme yields a high-resolution and monotone solution of the shallow-water equations [15, 22].

Hancock's method is a two-step scheme that is implemented in predictor-corrector fashion. In the predictor step, the primitive equations in generalized coordinates are solved to advance the solution to the half-time level. At the half-time level, the solution is reconstructed at cell faces using the Monotone Upwind Scheme for Conservation Laws (MUSCL) approach [23], and the fluxes are evaluated at cell faces by Roe's approximate Riemann solver [19]. In the corrector step, the interface fluxes and source terms evaluated at the half-time level are used to advanced the solution from the base time level to the next full time level using the discretized form of the integral equations (Equation 1). Boundary conditions are implemented by lining the exterior of the model domain with ghost cells, and specifying the depth and velocity in the ghost cells such that the desired boundary state is achieved upon calling the Riemann solver [15, 22].

NUMERICAL SOLUTION OF THE ADJOINT EQUATIONS

The adjoint shallow-water equations are solved by utilizing Roe's fluctuation-splitting method to directly update the solution without computing fluxes. This approach has previously been applied to solve conservation equations [20, 24]. Presented here are both a one-step and a two-step fluctuation-splitting scheme to solve the adjoint equations in generalized coordinates, which appear as

$$\frac{\partial \mathbf{\Phi}}{\partial \tau} + \mathbf{A}_{\Phi *} \frac{\partial \mathbf{\Phi}}{\partial \xi} + \mathbf{B}_{\Phi *} \frac{\partial \mathbf{\Phi}}{\partial \eta} + \mathbf{C}_{\Phi} \mathbf{\Phi} + \mathbf{D}_{\Phi} = 0 \tag{9}$$

and the matrices $\mathbf{A}_{\Phi *}$, and $\mathbf{B}_{\Phi *}$ are defined as

$$\mathbf{A}_{\Phi *} = \begin{pmatrix} 0 & (u^2 - a^2)\xi_x + uv\xi_y & uv\xi_x + (v^2 - a^2)\xi_y \\ -\xi_x & -(2u\xi_x + v\xi_y) & -v\xi_x \\ -\xi_y & -u\xi_y & -(u\xi_x + 2v\xi_y) \end{pmatrix} \tag{10}$$

$$\mathbf{B}_{\Phi *} = \begin{pmatrix} 0 & (u^2 - a^2)\eta_x + uv\eta_y & uv\eta_x + (v^2 - a^2)\eta_y \\ -\eta_x & -(2u\eta_x + v\eta_y) & -v\eta_x \\ -\eta_y & -u\eta_y & -(u\eta_x + 2v\eta_y) \end{pmatrix} \tag{11}$$

One-step fluctuation splitting approach

LeVeque has presented a one-step fluctuation splitting approach for solving systems of hyperbolic equations that, similar to the adjoint shallow-water equations, do not appear in conservative form [20]. Using this approach, fluctuations are used to directly compute the new values of $\mathbf{\Phi}$ in each cell. This is in contrast to the solution method for the shallow-water equations, where forward and backward moving fluctuations are used to compute interface fluxes. The direct updating of $\mathbf{\Phi}$ is achieved by splitting fluctuations $\mathbf{A}_{\Phi *}\Delta\mathbf{\Phi}$ into positive and negative moving waves as follows,

$$\mathbf{A}_{\Phi *}\Delta\mathbf{\Phi} = \mathbf{A}^{+}_{\Phi *}\Delta\mathbf{\Phi} + \mathbf{A}^{-}_{\Phi *}\Delta\mathbf{\Phi} \tag{12}$$

where $\mathbf{A}^{+}_{\Phi *}\Delta\mathbf{\Phi}$ represents the positive moving fluctuations, and $\mathbf{A}^{-}_{\Phi *}\Delta\mathbf{\Phi}$ represents the negative moving fluctuations. The matrices $\mathbf{A}^{+}_{\Phi *}$ and $\mathbf{A}^{-}_{\Phi *}$ are defined as,

$$\mathbf{A}^{\pm}_{\Phi *} = \mathbf{R}_{\Phi *}\mathbf{\Lambda}^{\pm}_{\Phi *}\mathbf{R}^{-1}_{\Phi *} \tag{13}$$

where $\mathbf{\Lambda}^{\pm}_{\Phi *}$ are the diagonal matrices containing the positive and negative eigenvalues of $\mathbf{A}_{\Phi *}$ and the columns of $\mathbf{R}_{\Phi *}$ contain the corresponding right eigenvectors. These are given by,

$$\mathbf{\Lambda}_{\Phi *} = \begin{pmatrix} -a\zeta - u_\xi & 0 & 0 \\ 0 & -u_\xi & 0 \\ 0 & 0 & a\zeta - u_\xi \end{pmatrix} \tag{14}$$

and

$$\mathbf{R}_{\Phi *} = \frac{1}{2a} \begin{pmatrix} a\zeta - u_\xi & -v_\xi & a\zeta + u_\xi \\ \xi_x & -\xi_y & -\xi_x \\ \xi_y & \xi_x & -\xi_y \end{pmatrix} \tag{15}$$

where $\zeta = \sqrt{\xi_x^2 + \xi_y^2}$, $u_\xi = u\xi_x + v\xi_y$ and $v_\xi = -u\xi_y + v\xi_x$.

With the matrix $\mathbf{B}_{\Phi*}$ split in an analogous manner, implementation of the fluctuation splitting approach leads to the following discretization when $\Delta\xi = \Delta\eta = 1$,

$$\mathbf{\Phi}_{j,k}^{n-1} = \mathbf{\Phi}_{j,k}^{n} - \Delta t[(\mathbf{A}_{\Phi*}^{+}\Delta\mathbf{\Phi})_{j-1/2,k}^{n} + (\mathbf{A}_{\Phi*}^{-}\Delta\mathbf{\Phi})_{j+1/2,k}^{n}(\mathbf{B}_{\Phi*}^{+}\Delta\mathbf{\Phi})_{j,k-1/2}^{n}$$

$$+ (\mathbf{B}_{\Phi*}^{-}\Delta\mathbf{\Phi})_{j,k+1/2}^{n}(\mathbf{C}_{\Phi}\mathbf{\Phi})_{j,k}^{n} + (\mathbf{D}_{\Phi})_{j,k}^{n}] \tag{16}$$

However, this scheme is only first-order accurate in space and time. Second-order accuracy is obtained by subtracting a correction term of the form

$$\Delta t[(\dot{\mathbf{F}}_{\Phi*j+1/2,k} - \dot{\mathbf{F}}_{\Phi*j-1/2,k}) + (\dot{\mathbf{G}}_{\Phi*j,k+1/2} - \dot{\mathbf{G}}_{\Phi*j,k-1/2})] \tag{17}$$

where

$$\dot{\mathbf{F}}_{\Phi*} = \tfrac{1}{2}(\mathbf{I} - \Delta t\mathbf{\Lambda}_{\Phi*})|\mathbf{\Lambda}_{\Phi*}|\Delta\mathbf{V}_{\Phi*} \tag{18}$$

and $\Delta\mathbf{V}_{\Phi*}$ represents the characteristic variables of $\mathbf{A}_{\Phi*}$. These are given by,

$$\Delta\mathbf{V}_{\Phi*} = \frac{1}{\zeta^2}\begin{pmatrix} \zeta\Delta\phi + (u\zeta + a\xi_x)\Delta\psi_x + (v\zeta + a\xi_y)\Delta\psi_y \\ -2a(\xi_y\Delta\psi_x - \xi_x\Delta\psi_y) \\ \zeta\Delta\phi + (u\zeta - a\xi_x)\Delta\psi_x + (v\zeta - a\xi_y)\Delta\psi_y \end{pmatrix} \tag{19}$$

An analogous term for $\dot{\mathbf{G}}_{\Phi*}$ can be determined using the eigenvalues, right eigenvectors, and characteristic variables of the matrix $\mathbf{B}_{\Phi*}$. These are the same as for $\mathbf{A}_{\Phi*}$ except that η_x and η_y replace ξ_x and ξ_y, respectively. Note that the wave strengths $\Delta\mathbf{V}_{\Phi*}$ in the second-order corrections must be limited to achieve a monotone solution [20].

Two-step fluctuation splitting approach

The adjoint shallow-water equations can alternatively be solved in a two-step scheme to achieve second-order accuracy. This approach is similar to Hancock's scheme that has been applied to solve the shallow-water equations [15, 22]. The first step of the two-step scheme predicts a solution to Equation (9) in cell j, k at $t - \Delta t/2$ as

$$\tilde{\mathbf{\Phi}}_{j,k} = \mathbf{\Phi}_{j,k}^{n} - \frac{\Delta t}{2}(\mathbf{A}_{\Phi*}\overline{\Delta\mathbf{\Phi}}_{\xi} + \mathbf{B}_{\Phi*}\overline{\Delta\mathbf{\Phi}}_{\eta} + \mathbf{C}_{\Phi}\mathbf{\Phi} + \mathbf{D}_{\Phi})_{j,k}^{n} \tag{20}$$

where the overbar denotes a cell average gradient of $\mathbf{\Phi}$, i.e.,

$$\begin{aligned} \overline{\Delta\mathbf{\Phi}}_{\xi_{j,k}} &= \mathrm{avg}(\mathbf{\Phi}_{j,k} - \mathbf{\Phi}_{j-1,k}, \mathbf{\Phi}_{j+1,k} - \mathbf{\Phi}_{j,k}) = \mathrm{avg}(\kappa_L, \kappa_R) \\ \overline{\Delta\mathbf{\Phi}}_{\eta_{j,k}} &= \mathrm{avg}(\mathbf{\Phi}_{j,k} - \mathbf{\Phi}_{j,k-1}, \mathbf{\Phi}_{j,k+1} - \mathbf{\Phi}_{j,k}) = \mathrm{avg}(\kappa_L, \kappa_R) \end{aligned} \tag{21}$$

There are many choices for the averaging function, $\mathrm{avg}(\kappa_L, \kappa_R)$, but linear averages will not preserve the monotonicity of the solution. Nonlinear averages have been specifically designed for such a purpose and have been termed flux or slope limiters [25]. These limiters preserve

monotonicity by becoming first-order accurate near discontinuities, yet remain second-order accurate in regions of smooth flow. In this study, the van Albada limiter is used,

$$\mathrm{avg}(\kappa_L, \kappa_R) = \frac{\kappa_L(\kappa_R^2 + \varepsilon) + \kappa_R(\kappa_L^2 + \varepsilon)}{\kappa_L^2 + \kappa_R^2 + 2\varepsilon} \tag{22}$$

Half-time level values to the left and right of each cell face are computed using the MUSCL reconstruction. Upwinding is then performed to compute the average value of $\mathbf{\Phi}$ for each face at the half-time level. For example, in the ξ direction the eigenvalues of the matrix $\mathbf{A}_{\Phi *}$ are used to determine the upwind direction for each wave. At the right face this yields,

$$\mathbf{\Phi}_{j+1/2,k}^{n-1/2} = \tfrac{1}{2}(\tilde{\mathbf{\Phi}}_{j+1/2,k}^{L} + \tilde{\mathbf{\Phi}}_{j+1/2,k}^{R} - |\bar{\mathbf{A}}_{\Phi *}|\bar{\mathbf{A}}_{\Phi *}^{-1}(\tilde{\mathbf{\Phi}}_{j+1/2,k}^{R} - \tilde{\mathbf{\Phi}}_{j+1/2,k}^{L})) \tag{23}$$

which can be rewritten as

$$\mathbf{\Phi}_{j+1/2,k}^{n-1/2} = \tfrac{1}{2}(\tilde{\mathbf{\Phi}}_{j+1/2,k}^{L} + \tilde{\mathbf{\Phi}}_{j+1/2,k}^{R} - \bar{\mathbf{R}}_{\Phi *}|\bar{\mathbf{\Lambda}}_{\Phi *}|\bar{\mathbf{\Lambda}}_{\Phi *}^{-1}\Delta\bar{\mathbf{V}}_{\Phi *}) \tag{24}$$

where the overbar denotes the arithmetic average of MUSCL reconstructed data across the cell face. A similar expression is employed for cell faces with normal vectors in the η direction using the matrix $\mathbf{B}_{\Phi *}$. In the second step of the two-step scheme, the solution is computed at the next full time level,

$$\begin{aligned}\mathbf{\Phi}_{j,k}^{n-1} = \mathbf{\Phi}_{j,k}^{n} - \Delta t[&\mathbf{A}_{\Phi * j,k}^{n-1/2}(\mathbf{\Phi}_{j+1/2,k}^{n-1/2} - \mathbf{\Phi}_{j-1/2,k}^{n-1/2}) \\ &+ \mathbf{B}_{\Phi * j,k}^{n-1/2}(\mathbf{\Phi}_{j,k+1/2}^{n-1/2} - \mathbf{\Phi}_{j,k-1/2}^{n-1/2}) + \mathbf{C}_{\Phi j,k}^{n-1/2}\tilde{\mathbf{\Phi}}_{j,k} + \mathbf{D}_{\Phi j,k}^{n-1/2}]\end{aligned} \tag{25}$$

where $\mathbf{A}_{\Phi * j,k}^{n-1/2}$, $\mathbf{B}_{\Phi * j,k}^{n-1/2}$, $\mathbf{C}_{\Phi * j,k}^{n-1/2}$, and $\mathbf{D}_{\Phi * j,k}^{n-1/2}$ are computed as the arithmetic averages of time levels n and $n-1$. This information, which results from solving the shallow-water equations, must be recalled from a file or internal memory at each time level to permit the solution of the adjoint shallow-water equations.

Boundary conditions

Boundary conditions are implemented by placing appropriate values of $\mathbf{B}_{\Phi}$ in ghost cells adjacent to the boundary. Wall boundaries are implemented at corresponding wall boundaries in the direct problem and are achieved by setting the adjoint variables ψ_x and ψ_y in the ghost cell such that the component perpendicular to the boundary is zero while the parallel component is identical to that of the first interior cell. This leads to the following conditions

$$(\psi_x)_{\mathrm{g}} = (\psi_x)_{\mathrm{d}}(\sin^2\alpha - \cos^2\alpha) - 2(\psi_y)_{\mathrm{d}}\sin\alpha\cos\alpha \tag{26}$$

$$(\psi_y)_{\mathrm{g}} = -2(\psi_x)_{\mathrm{d}}\sin\alpha\cos\alpha + (\psi_y)_{\mathrm{d}}(\cos^2\alpha - \sin^2\alpha) \tag{27}$$

where the subscripts g and d refer to the ghost and domain cells, respectively. The variable, ϕ, is zero-order extrapolated from the flow domain while the gradients in the direction perpendicular are zero-order extrapolated.

Open boundaries are implemented at inflow and outflow boundaries and are achieved by linearly extrapolating the adjoint variables to the ghost cells while zero-order extrapolating the gradients.

ONE-DIMENSIONAL RESULTS

Problem description

The proposed numerical schemes for the adjoint shallow-water equations are first tested on a one-dimensional problem with an exact solution. The one-dimensional version of the direct and adjoint problems can be obtained by simply dropping all terms in Equations (1) and (6), respectively, that are associated with variables or gradients in the y-direction and by assuming Ω is a one-dimensional space.

For unsteady flow, an exact solution to the adjoint equations cannot be obtained because wave speed and velocity, which must be evaluated numerically, appear as coefficients in the adjoint problem. However, for the special case of steady, frictionless, uniform flow over a horizontal bed, an exact solution to the adjoint equations is possible.

This numerical test is based upon a problem in which steady flow conditions exist in a channel of length L, over a duration, T, with depth $h(x,t)=h_o$ and velocity $u(x,t)=u_o$. The measuring function appearing in Equation (4) is specified as,

$$r(h)=\tfrac{1}{2}(h(x,t)-\bar{h})^2\delta(x-x_o) \tag{28}$$

where $\bar{h}$ is a desired or measured depth at the monitoring location, x_o. This choice for r yields a point source of constant magnitude in the adjoint problem, which is given by

$$\frac{\partial r}{\partial h}=(h(x,t)-\bar{h})\delta(x-x_o) \tag{29}$$

where $\delta(\ )$ is the Dirac delta function. The resulting adjoint problem solution is then given as follows [18],

$$V_{\Phi 1}=\begin{cases}\dfrac{h_o-\bar{h}}{u+c} & \text{if } x_o+\lambda_1\tau<x<x_o \\ 0 & \text{otherwise}\end{cases} \tag{30}$$

$$V_{\Phi 2}=\begin{cases}\dfrac{h_o-\bar{h}}{-u+c} & \text{if } x_o<x<x_o+\lambda_2\tau \\ 0 & \text{otherwise}\end{cases} \tag{31}$$

where $V_{\Phi 1}=\phi+(u+a)\psi_x$ and $V_{\Phi 2}=\phi+(u-a)\psi_x$ are the characteristic variables of the adjoint equations, which are associated with the wave speeds $\lambda_1=-u-a$ and $\lambda_2=-u+a$, respectively.

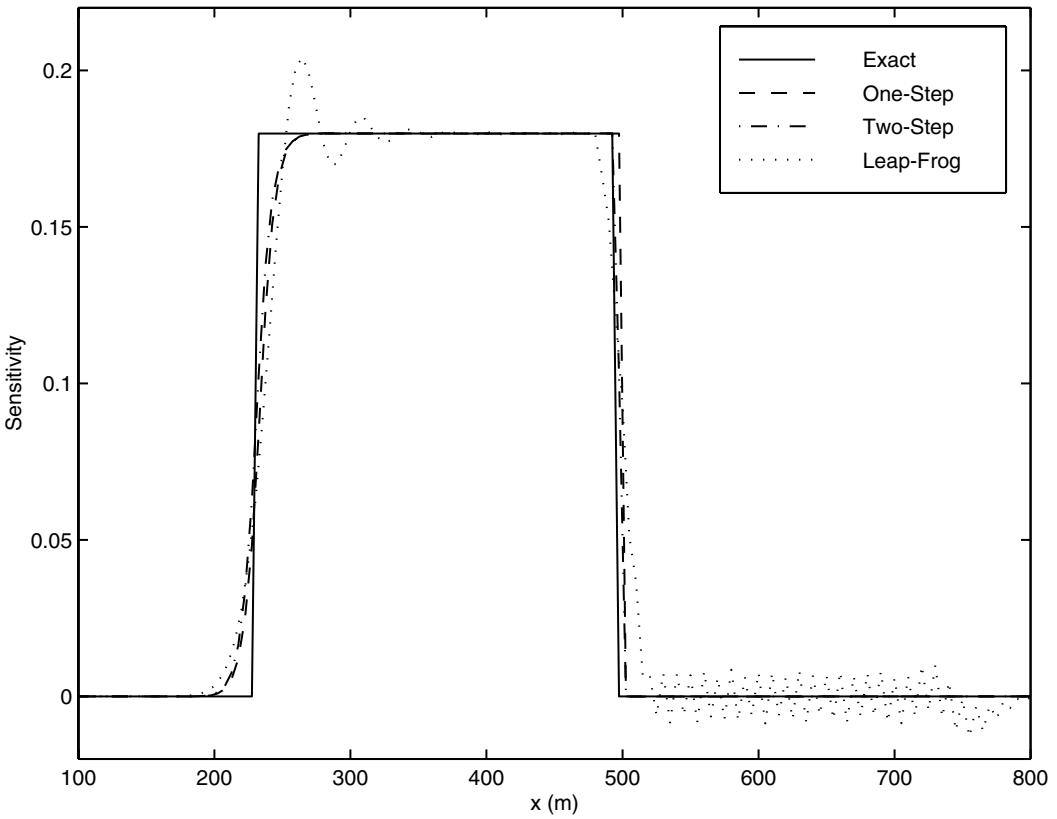

Figure 1. Riemann invariant $V_{\Phi 1}(x, 352.0\,\mathrm{s})$.

Both the one-step and two-step methods are applied to solve this problem. In addition, this adjoint problem solution contains discontinuities and therefore represents an excellent test for the numerical schemes presented here.

Numerical test

Using $L = 1000\,\mathrm{m}$, $T = 400\,\mathrm{s}$, $h_o = 2.0\,\mathrm{m}$, $u_o = 1.131\,\mathrm{m\,s^{-1}}$, $\bar{h} = 1.0\,\mathrm{m}$, and $x_o = 500\,\mathrm{m}$, the test problem is solved using the one-step, two-step, and leap-frog schemes, which has previously been applied to solve the adjoint shallow-water equations [10]. A constant cell length, $\Delta x = 5\,\mathrm{m}$ and time step, $\Delta t = 0.5\,\mathrm{s}$ are used. To compare the performance of the three methods, the Riemann invariants $V_{\Phi 1}$ and $V_{\Phi 2}$ evaluated at $t = 352.0\,\mathrm{s}$ are shown in Figures 1 and 2, respectively. From the figures it is seen that the one-step and two-step schemes achieve a monotone solution with minimal numerical dissipation. In addition, both schemes yield nearly identical solutions that compare well with the exact solution. In contrast, the leap-frog scheme develops oscillations at the advancing front, located at $x \simeq 230\,\mathrm{m}$ in Figure 1 and at $x \simeq 650\,\mathrm{m}$ in Figure 2. The leap-frog scheme also develops oscillations at the stationary front, located at $x = 500\,\mathrm{m}$ in both figures. The oscillations at $x = 500\,\mathrm{m}$ are due to

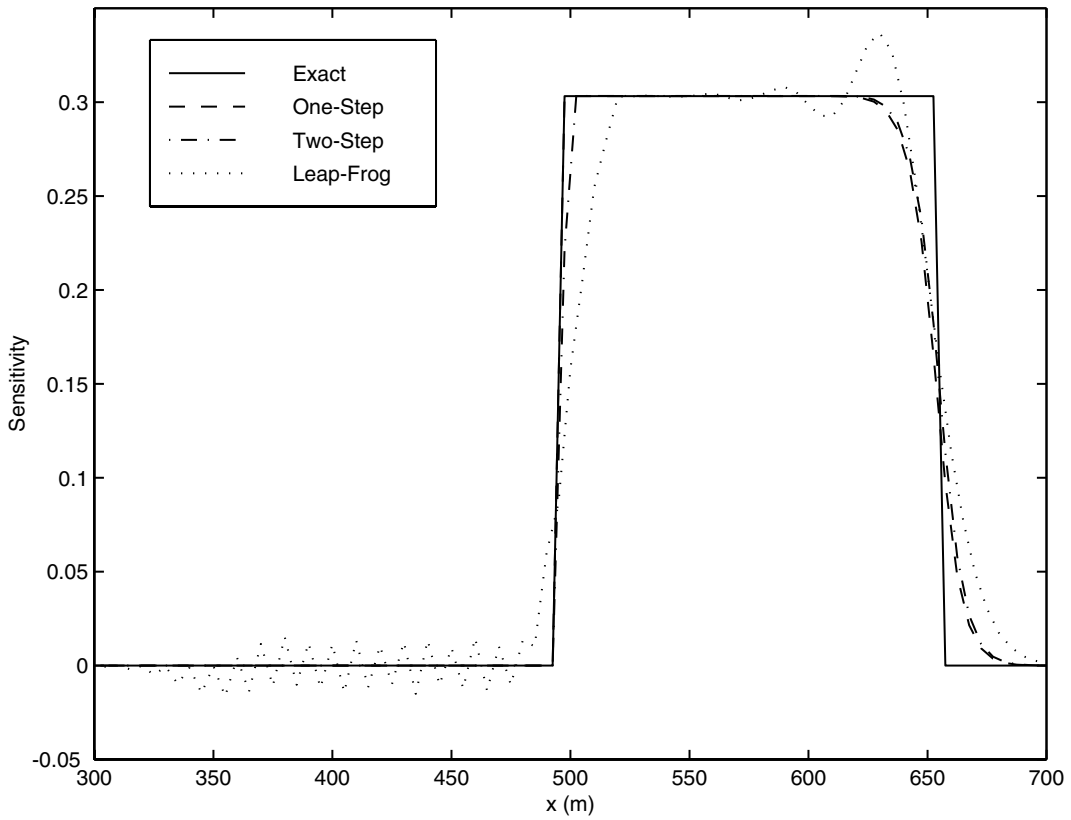

Figure 2. Riemann invariant $V_{\Phi 2}(x, 352.0\,\mathrm{s})$.

the decoupling of the solution between the odd and even grid points, which is a common shortcoming of the leap-frog scheme. The results of these tests reveal that the fluctuation-splitting-based schemes yield a far superior solution than the leap-frog scheme. Neither the one-step nor two-step scheme is shown to be superior to the other in terms of accuracy for this example. However, analysis in the next section reveals cases where the two-step method is preferred.

Numerical analysis

The previous test problem revealed that the one-step and two-step schemes achieved a similar level of accuracy in a test problem with uniform wave speeds. However, analysis of each scheme applied to the scalar advection problem reveals that the two-step method yields more accurate solutions in the presence of unsteady wave speeds, which often occur in open channel flow. Consider the simple problem of a scalar being advected in one dimension,

$$\frac{\partial c}{\partial t} + u\frac{\partial c}{\partial x} = 0 \tag{32}$$

where c represents the scalar and u is the advection velocity. The solution of this equation in cell j at time level $n+1$ can be obtained from the forward in time Taylor series, which is written as

$$c_j^{n+1} = c_j^n + \Delta t \frac{\partial c_j^n}{\partial t} + \frac{\Delta t^2}{2} \frac{\partial^2 c_j^n}{\partial t^2} + O(\Delta t^3) \tag{33}$$

where Δt denotes the time increment. With the aid of Equation (32) and the chain rule of differentiation, Equation (33) can be written as

$$c_j^{n+1} = c_j^n - \Delta t u_j^n \frac{\partial c_j^n}{\partial x} - \frac{\Delta t^2}{2} \left\{ \frac{\partial u_j^n}{\partial t} \frac{\partial c_j^n}{\partial x} - u_j^n \frac{\partial}{\partial x} \left(u_j^n \frac{\partial c_j^n}{\partial x} \right) \right\} + O(\Delta t^3) \tag{34}$$

For the case where $u > 0$, but may be unsteady and nonuniform in x, the one-step method yields the following approximation for c_j^{n+1},

$$c_j^{n+1} = c_j^n - \Delta t u_{j-1/2}^n \left(\frac{c_j^n - c_{j-1}^n}{\Delta x} \right) - \frac{\Delta t}{2} \left(\frac{u_{j+1/2}^n \overline{\Delta c}_{j+1/2} - u_{j-1/2}^n \overline{\Delta c}_{j-1/2}}{\Delta x} \right)$$

$$+ \frac{\Delta t^2}{2\Delta x} \left(\frac{(u_{j+1/2}^n)^2 \overline{\Delta c}_{j+1/2} - (u_{j-1/2}^n)^2 \overline{\Delta c}_{j-1/2}}{\Delta x} \right) \tag{35}$$

where Δx represents the length of a computational cell and all cells are assumed to be equal in length. The second term on the right side of this equation is an upwind approximation to $u_j^n \partial c_j^n / \partial x$, while the third term increases the spatial accuracy of this approximation. In order to see this, assume $\overline{\Delta c}_{j-1/2} = c_j^n - c_{j-1}^n$ and $\overline{\Delta c}_{j+1/2} = c_{j+1}^n - c_j^n$. Equation (35) can then be written as

$$c_j^{n+1} = c_j^n - \frac{\Delta t}{2} \left\{ u_{j-1/2}^n \left(\frac{c_j^n - c_{j-1}^n}{\Delta x} \right) + u_{j+1/2}^n \left(\frac{c_{j+1}^n - c_j^n}{\Delta x} \right) \right\}$$

$$+ \frac{\Delta t^2}{2\Delta x} \left\{ (u_{j+1/2}^n)^2 \left(\frac{c_{j+1}^n - c_j^n}{\Delta x} \right) - (u_{j-1/2}^n)^2 \left(\frac{c_j^n - c_{j-1}^n}{\Delta x} \right) \right\} \tag{36}$$

The approximation to $u_j^n \partial c_j^n / \partial x$ is now an average of the values at the left and right cell faces and is therefore second order accurate with respect to Δx. The third term is a space-centered approximation to $(u_j^n)^2 \partial^2 c_j^n / \partial x^2$, which is not entirely appropriate as shown by Equation (34) and in fact introduces an error proportional to $u_j^n (\partial u_j^n / \partial x)(\partial c_j^n / \partial x)$. Therefore, this approximation is only appropriate when u is uniform. In addition, the one-step method does not yield an approximation to the term $(\partial u_j^n / \partial t)(\partial c_j^n / \partial x)$, which is nonzero when u is unsteady.

The two-step method yields the following approximation to c_j^{n+1},

$$c_j^{n+1} = c_j^n - \Delta t u_j^{n+1/2}\left(\frac{c_j^n - c_{j-1}^n}{\Delta x}\right) - \frac{u_j^{n+1/2}\Delta t}{2}\left(\frac{\overline{\Delta c}_j - \overline{\Delta c}_{j-1}}{\Delta x}\right) + \frac{u_j^{n+1/2}\Delta t^2}{2\Delta x}\left(\frac{u_j^n\overline{\Delta c}_j - u_{j-1}^n\overline{\Delta c}_{j-1}}{\Delta x}\right) \tag{37}$$

Once again, the second term is an upwind approximation to $\partial c_j^n/\partial x$, while the third term increases the spatial accuracy of this approximation. In this case assume $\overline{\Delta c}_j = c_{j+1}^n - c_j^n$ and $\overline{\Delta c}_j = c_j^n - c_{j-1}^n$, then Equation (37) can be written as,

$$c_j^{n+1} = c_j^n - \Delta t u_j^{n+1/2}\left(\frac{c_{j+1}^n - c_{j-1}^n}{2\Delta x}\right) + \frac{u_j^{n+1/2}\Delta t^2}{2\Delta x}\left\{u_j^n\left(\frac{c_{j+1}^n - c_j^n}{\Delta x}\right) - u_{j-1}^n\left(\frac{c_j^n - c_{j-1}^n}{\Delta x}\right)\right\} \tag{38}$$

Furthermore, substituting $u^{n+1/2} = (u^n + u^{n+1})/2$, yields

$$c_j^{n+1} = c_j^n - \Delta t u_j^n\left(\frac{c_{j+1}^n - c_{j-1}^n}{2\Delta x}\right) - \frac{\Delta t^2}{2}\left(\frac{u_j^{n+1} - u_j^n}{\Delta t}\right)\left(\frac{c_{j+1}^n - c_{j-1}^n}{2\Delta x}\right) + \frac{u_j^n\Delta t^2}{2\Delta x}\left\{u_j^n\left(\frac{c_{j+1}^n - c_j^n}{\Delta x}\right) - u_{j-1}^n\left(\frac{c_j^n - c_{j-1}^n}{\Delta x}\right)\right\} + O(\Delta t^3) \tag{39}$$

The approximation to $u_j^n\partial c_j^n/\partial x$ is centered at j and is therefore second order accurate with respect to Δx. The fourth term on the right is an approximation to $u_j^n\partial(u_j^n\partial c_j^n/\partial x)/\partial x$, although u is upwind biased within the gradient operator. This also introduces an error proportional to $u_j^n(\partial u_j^n/\partial x)(\partial c_j^n/\partial x)$ and therefore both the one- and two-step methods are equally deficient in this regard. However, the third term on the right side of Equation (39) is an approximation to $(\partial u_j^n/\partial t)(\partial c_j^n/\partial x)$, which the one-step method lacked. Therefore, the two-step method is expected to yield more accurate solutions when u is unsteady. Note that when u is steady and uniform, both methods yield an identical an approximation to c_j^{n+1}, and the approximation is consistent with Equation (34) through order $O(\Delta t^2)$. In addition, the two-step method introduces a term that is $O(\Delta t^3)$, which is not specifically written in Equation (39).

In order to investigate the accuracy of the two methods, a simple case is solved in which u is unsteady and nonuniform and the initial condition is given by $c(x,0) = \sin(\pi x/L)$. The advection velocity is given by $u(x,t) = 0.1xt$, while $\Delta t = 0.14$ s, $\Delta x = 10$ m, and open boundary conditions are specified at both ends of the domain. The exact solution in this case is $c(x,t) = \sin(\pi x e^{-0.05t^2}/L)$, where $L = 100$ m is the length of the domain. Figure 3 compares

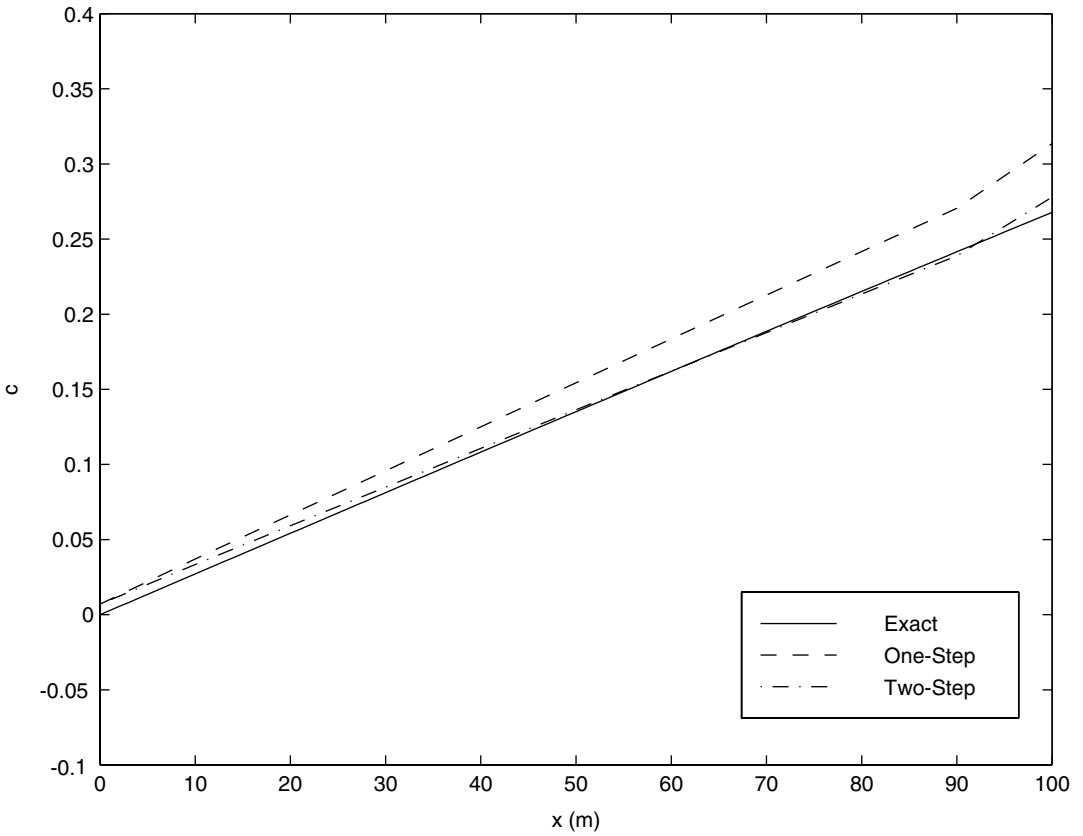

Figure 3. Comparison of one- and two-step methods with the exact solution for scalar advection with unsteady velocity.

the one- and two-step solutions with the exact solution at $t = 7$ s. The two-step solution is much more accurate than the one-step prediction in this case. Both methods yield solutions of similar accuracy when u is steady, but nonuniform. However, the two-step method is more modular in design and is therefore more attractive from a model development standpoint. Therefore, the two-step method is preferred over the one-step scheme. The performance of the two-step scheme in generalized two-dimensional coordinates is evaluated next.

TWO-DIMENSIONAL RESULTS

A pair of parameter identification problems are used to evaluate the performance of the two-step scheme in two-dimensional space. The solution to the adjoint problem yields a gradient vector that represents the sensitivity of an objective function to a parameter vector. This information can be used to perform gradient based optimization, as is described next.

Flood characterization problem

Parameters describing the time evolution of the inflow discharge to an idealized, meandering, river reach are first optimized using hypothetical depth measurements made at a monitoring station within the solution domain. Knowledge of the inflow discharge could then permit real-time, short-term forecasts of hydrodynamic conditions in additional channel reaches downstream. In practice, the monitoring station would supply real-depth data to an optimization algorithm, which would then find an estimate for the unsteady, inflow, discharge to the reach. However, in this problem, depth data from a model simulation using the known inflow discharge are used in place of real measurements. This approach is the best technique for examining the performance of the proposed numerical scheme because errors associated with the forward problem solution do not arise in this situation [3, 4].

It is assumed that the initial condition for the control period is known as a result of a forecast from a previous time period, so additional parameters associated with the initial condition are not identified. Furthermore, the initial flow is assumed to be steady for the sake of simplicity. A non-reflecting boundary is employed at the downstream end of the channel reach in the direct problem, which permits water waves to pass freely to subsequent channel reaches. An additional sampling station could alternatively be placed at the downstream end of the channel reach to supply the boundary condition, but this approach would not yield additional insight into the proposed model's performance. The benefit of constructing the numerical tests in the proposed manner is that the ability of the method to accurately compute adjoint variables can be evaluated based on the convergence of the optimization algorithm. This is because the adjoint variables are used to compute the objective function gradient information, which is used by the optimization algorithm to obtain a converged parameter space. However, the parameter space will not converge unless the objective function gradients, and therefore the adjoint variables, are accurately determined. Therefore, convergence of the parameter space reflects the accuracy of the adjoint solution.

The objective is to identify the total discharge at the inflow boundary, $Q(t)$, that leads to minimizing the difference between the model predicted depth at the monitoring station, $h(x_o, y_o, t)$ and the measured depth $\bar{h}(t)$. A least-squares measuring function is used in this case, which has the form,

$$r(h) = \tfrac{1}{2}(h(x, y, t) - \bar{h}(t))^2 \delta(x - x_o, y - y_o) \tag{40}$$

where $\delta(\,)$ is the two-dimensional Dirac delta function. The objective function is minimized by optimizing the discharge at the upstream boundary at m selected time levels over the control period, T. Therefore, the discharges at m time levels form an m-dimensional parameter space to be optimized. Linear interpolation is used to determine the discharge at all other times.

An unconstrained optimization algorithm known as CONMIN is utilized to estimate the parameter space [26]. CONMIN is a gradient-based optimization method that has performed well for similar optimization problems [3, 4, 8, 10]. It permits the use of either the conjugate gradient method or a variable metric method utilizing a Broyden, Fletcher, Goldfarb, and Shanno (BFGS) update [27]. First, an initial guess for the unknown parameters is made and the direct problem is solved in the forward time direction over period, T, which yields the resulting hydrodynamic conditions in the channel and the objective function, J. Next, the adjoint problem is solved in the reverse time direction to determine the gradient of J with respect to the m-dimensional parameter space. CONMIN then computes a new estimate for

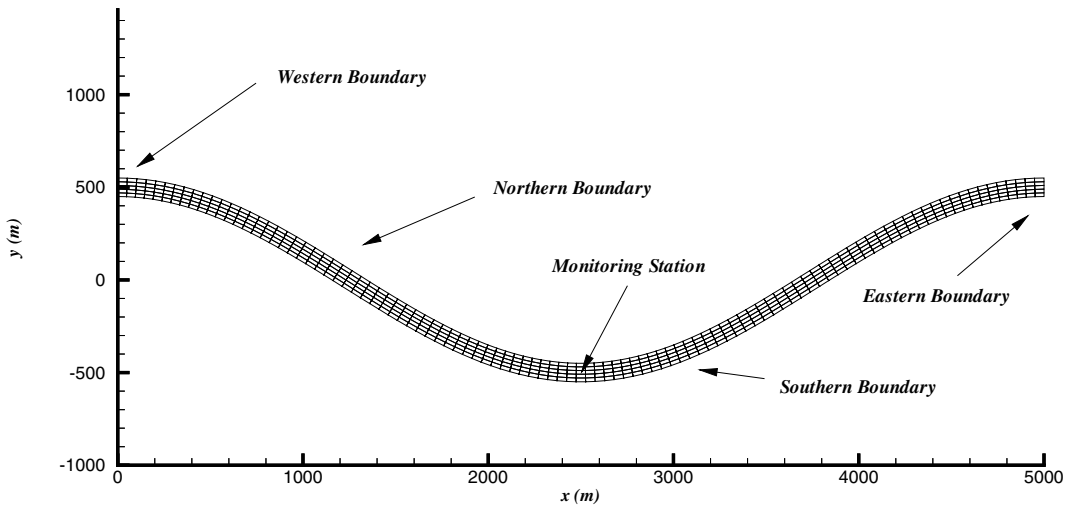

Figure 4. Two-dimensional domain and computational grid used in the flood characterization problem.

the unknown m-dimensional parameter space using J and its gradient. This procedure repeats itself until the objective function is minimized.

Given that the boundary condition $\psi_x = 0$ is enforced at the western boundary of the domain, the gradient of the objective function with respect to the m-dimensional parameter space is given as [17],

$$\frac{\delta J}{\delta Q(t_m)} = \int_{\mathscr{W}} \phi(x, y, t_m)\, \mathrm{d}\mathscr{W} \tag{41}$$

where $\mathscr{W}$ denotes the western (inflow) boundary of the domain and t_m represents the perturbation time.

The channel geometry is chosen to be sinusoidal in shape to examine the multi-directional wave propagation properties of the proposed scheme. The channel geometry is presented in Figure 4 and is given by,

$$y_c(x) = A\cos(2\pi x/L) \tag{42}$$

where y_c is the y-coordinate of the channel centerline, x is distance in the easterly direction, L is the length of the channel reach in the easterly direction, and A is the amplitude of the oscillations in the channel centerline. The channel is assumed to have a constant width, W, and a parabolic shape at each cross-section. In addition, the flood plain is assumed to have a constant slope in the easterly direction. The elevation of the channel bottom above an arbitrary datum is given by,

$$z(x, y) = \Delta z - \frac{\Delta z}{L}x + \gamma l(x, y)^2 \tag{43}$$

where Δz is the change in elevation of the flood plain in the easterly direction, γ is a parameter that describes the parabolic shape of the channel cross-section, and $l(x, y)$ is the length of a vector that is normal to the channel centerline and passes through (x, y).

For the following tests, the preceeding parameters describing the channel geometry are given as, $L = 5000\,\mathrm{m}$, $A = 500\,\mathrm{m}$, $W = 100\,\mathrm{m}$, $\Delta z = 1\,\mathrm{m}$, $n = 0.015$, and $\gamma = 8 \times 10^{-5}$. The channel is discretized by 100 quadrilateral cells in the ξ direction and five cells in the η direction, as shown in Figure 4. The monitoring station is positioned along the centerline of the channel and at its midpoint, as shown in Figure 4. This cell is indexed by $j = 51$ and $k = 3$. The initial steady flow in the channel is determined by specifying the depth in the ghost cells outside the western and eastern boundaries and allowing the solution to integrate to a steady state. The depth in the ghost cells is given by,

$$h_{0,k} = 3.5 - \frac{\Delta z}{L} x^c_{0,k} - z^c_{0,k} \ \text{(m)} \tag{44}$$

$$h_{N_\xi+1,k} = 3.5 - \frac{\Delta z}{L} x^c_{N_\xi+1,k} - z^c_{N_\xi+1,k} \ \text{(m)} \tag{45}$$

where the superscript c indicates cell *centers*. In general, shallow-water flow solutions require that the discharge be specified at the inflow boundary while the depth is specified at the outflow boundary to yield a well-posed problem. However, the Riemann solver that is built into the finite volume shallow-water model allows the inflow discharge and momentum fluxes to be computed subsequent to specifying the depth, thus yielding a stable numerical solution. A time step, $\Delta t = 2\,\mathrm{s}$, was used to integrate the equations in time.

The flux entering each inflow boundary cell was specified in terms of the total discharge at each time level $Q(t_m)$ using a discrete distribution function. Hence, $p_{0,k}\Delta s_{1,k} = w_k Q(t_m)$ where w is a distribution function with the property that,

$$\sum_{k=1}^{N_\eta} w_k = 1 \tag{46}$$

and $\Delta s_{1,k}$ is the length of the kth cell face located along the inflow boundary. The distribution function w_k for each inflow cell was determined by the steady-state discharge.

Using an inflow function given by,

$$Q(t) = Q_o f(t) \tag{47}$$

where $Q_o = 247\,\mathrm{m^3\,s^{-1}}$ is the steady-state discharge, and $f(t)$ is an amplification function, the *measured* depth at the monitoring location, $\bar{h}(t)$ is obtained by integrating the direct problem over a control period of duration, $T = 1000\,\mathrm{s}$. Subsequently, the proposed algorithm is applied to replicate the inflow discharge using only the measured depth, $\bar{h}(t)$. This procedure is first applied using an amplification function given by,

$$f(t) = \begin{cases} 1 + 2\sin(\pi t/600) & \text{if } t \leqslant 600 \\ 0 & \text{if } t > 600 \end{cases} \tag{48}$$

Using an initial guess given by $Q(t_m) = Q_o$ for $m = 1, \ldots, 50$, the optimization algorithm is applied to estimate the discharge at 50 of the 500 time levels in the numerical solution, while the remainder are linearly interpolated.

Initially, the objective function registers a value of $J = 134\,\mathrm{m^2\,s^{-1}}$. After 30 iterations, the objective function has been reduced to $J = 0.7\,\mathrm{m^2\,s^{-1}}$, and after 100 iterations, the objective

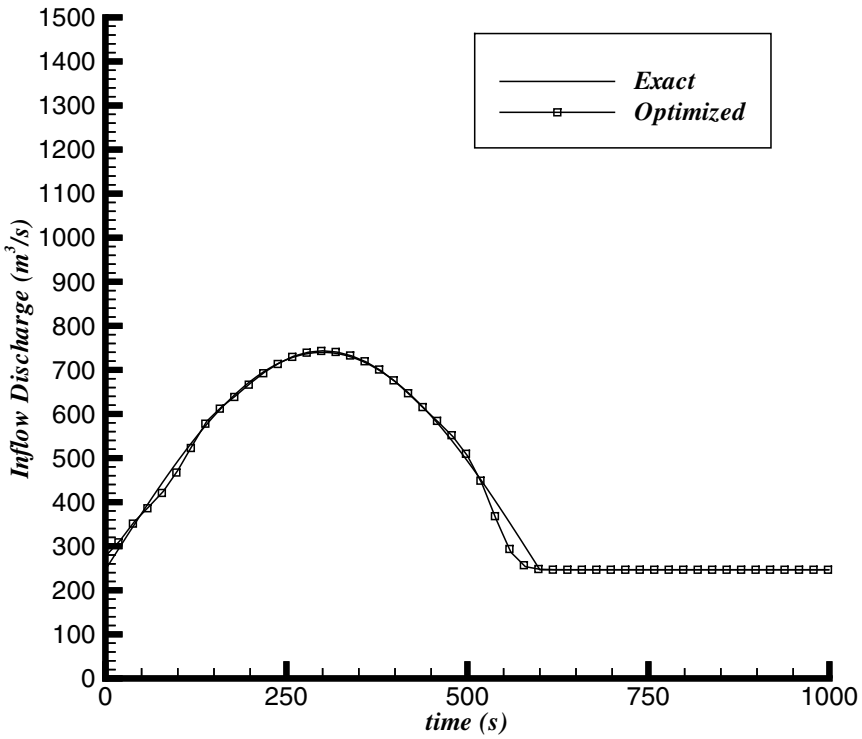

Figure 5. Optimized values of the inflow discharge for the first test compared to the exact values.

function has been reduced to $J = 0.06\,\mathrm{m}^2\,\mathrm{s}^{-1}$. A plot of the optimized inflow discharge after 100 iterations is presented in Figure 5, which shows that the estimated discharge has converged to the actual inflow. This implies that adjoint variable information is accurately propagated from the monitoring station to the western boundary, and reveals that the fluctuation splitting two-step approach performs well on an irregular domain in the presence of both variable bathymetry and bottom friction described by the Manning equation.

In the preceding test, each iteration of the optimization algorithm required approximately 15 s of computational time on a 300 MHz P2 workstation. Consequently, the optimization algorithm required approximately 450 s to reduce the objective function to a value less than 1.0, and 1500 s to reduce the objective function to a value less than 0.1. Comparing the optimization times with the duration of the control period, $T = 1000\,\mathrm{s}$, it can be concluded that the time required to determine the inflow discharge in a channel reach is on the order of the sampling time. Therefore, it is feasible to apply the proposed method in real-time to forecast hydraulic conditions.

In several tests not shown here, the parameter space was initially found to become trapped at local minima after roughly 20 iterations when either the conjugate gradient or BFGS option in CONMIN was utilized. However, utilizing five successive calls to CONMIN, the parameter space was found to reach the global minima within an acceptable tolerance. Consequently, an approach permitting five successive calls to CONMIN, each permitting a maximum of 20

iterations, is adopted for this and the following test. The conjugate gradient option is selected for the first four calls, while the BFGS option is selected for the final call, since variable metric methods perform best near the minima.

This procedure is repeated using an amplification function given by,

$$f(t)=\begin{cases}1+4\sin(\pi t/600) & \text{if } t\leqslant 600\\ 0 & \text{if } t>600\end{cases} \tag{49}$$

In this case, the peak inflow discharge exceeds that of the previous case by approximately 67 per cent, which creates a water wave that steepens as it travels downstream as a result of nonlinearity in the shallow-water equations. The initial guess is again given by $Q(t_m)=Q_o$ for $m=1,\ldots,50$, and the initial computed objective function value is $J=493\ \mathrm{m^2\ s^{-1}}$. However, convergence is not as rapid as in the previous case. The objective function is reduced to $J=47\mathrm{m^2 s^{-1}}$ after 30 iterations and $J=0.68\mathrm{m^2 s^{-1}}$ after 100 iterations. This test represents the more difficult of the two examples because the water wave propagation is strongly nonlinear, which causes the flood wave to steepen and eventually become discontinuous. Recall that the adjoint equations are linearized about the solution of the shallow-water equations. Improvement in the adjoint solution will only occur with an improved solution of the direct problem. However, in the presence of sharp fronts, numerical dissipation is added to the direct solution, which degrades its accuracy as well as the accuracy of the adjoint solution. Consequently, further convergence of the parameter space is not achieved, which explains the relatively poorer performance of the method in this case. Nevertheless, the optimized discharge after 100 iterations compares well with the actual discharge, as shown in Figure 6. Hence, the fluctuation splitting, two-step algorithm is again found to accurately propagate adjoint variable information in this more difficult example.

Solitary wave characterization problem

Next, the scheme is applied to identify parameters describing the time evolution of water surface elevation for the purpose of characterizing the wave form (wave height and effective period) of a tsunami-like long wave. The optimization problem is derived from a laboratory study conducted at the Waterways Experiment Station in the United States [28]. In this study, a conical island 0.625-m high with a base diameter equal to 7.2 m and a top diameter of 2.2 m was constructed in a laboratory tank that was 30-m wide and 25-m long. The center of the island was located at $x=13$ m and $y=15$ m, and the tank was filled to a level of 0.32 m with water. A wave generator was placed along the y-axis of the tank and was operated to generate a soliton that propagated in the positive x-direction. A sketch of the system is shown in Figure 7.

Here, the goal is to evaluate incident wave form using gage data collected in the vicinity of the island, where the wave is subject to shoaling, refraction, and diffraction. An objective function that is proporational to the misfit between measured and modeled values of depth at a set of gages is used, so the measuring function is specified as,

$$r(h)=\frac{1}{2}\sum_{k=1}^{N^g}(h(x,y,t)-h_k^g(t))^2\delta(x-x_k^g,y-y_k^g) \tag{50}$$

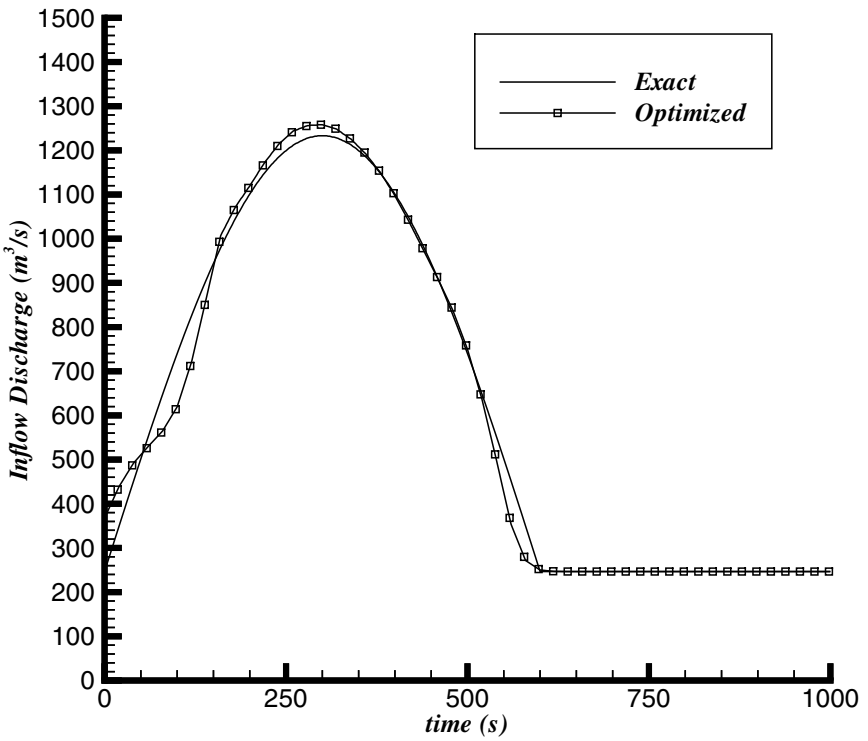

Figure 6. Optimized values of the inflow discharge for the second test compared to the exact values.

where (x_k^g, y_k^g) represents the coordinates of the kth gage and h_k^g represents the depth measured at the kth gage. Hence, an incident wave is sought with the property that it minimizes the difference between measured and modeled depths at a set of gages in the wave tank.

This is not an ideal test for the accuracy of the model since the solitary wave is dispersive while the model is non-dispersive. Nevertheless, previous studies have shown that shallow-water models give an accurate prediction of the near-field changes in depth around the island given the far-field wave condition [22, 29, 30]. To focus this test on the performance of the two-step scheme for solving the adjoint equations, and not the forward scheme's ability to resolve a dispersive wave, the depth measurements h_k^g are obtained from a solution of the direct problem instead of using laboratory measurements. This is consistent with the previous optimization problem. There are additional challenges associated with using laboratory or field measurements instead of numerical measurements, but this is outside the scope of this paper.

In the model, the domain is discretized by square cells with a side length equal to 0.2 m and a time step of 0.04 s of used to obtain the predicted values of depth. The model grid is shown in Figure 7. The incident wave is characterized in the model by a parameter vector that contains the depth as a function of time $h_w(t)$ along the y-axis. Hence, we assume that the incident wave is in the x-direction for simplicity. The parameter vector is given by the depth at every time step in the model between $t = 8$ s and $t = 12$ s, so the parameter space is of dimension 100 based on a time step of 0.04 s. Specifying ψ_x to be zero on the inflow

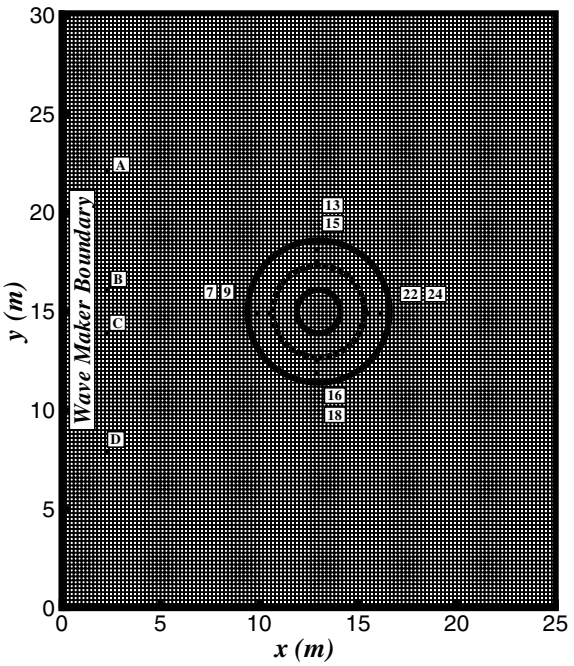

Figure 7. Plan view of the wave basin used for the solitary wave characterization problem. Solid circles in the center represent the top and bottom of the conical island. Dashed line in the center represents the still water level. Black squares represent monitoring stations. Gage numbers and letters are shown. The numbered gages are those used by Briggs *et al.* [28], while the lettered gages are introduced here for analysis purposes.

boundary, the sensitivity of the objective function to perturbations of the parameter vector and is given by [17],

$$\frac{\delta J}{\delta h_w(t_m)} = \int_{\Gamma_w} \phi(u+c)|_{t_m} \, \mathrm{d}\Gamma_w \tag{51}$$

CONMIN is applied to optimize the parameter space as was done in the previous test. In each optimization problem, CONMIN is called five times whereby the conjugate gradient option is selected in the first four calls and the BFGS option is selected in the final call. Furthermore, each call to CONMIN is limited to 20 objective function calls. Hence, the forward and adjoint problems are each solved 100 times and the total computational time in this case is approximately 400 min on a 700 MHz PIII workstation. The computational times are considerably larger in this case than in the flood wave problem because 18 750 cells are used in the solitary wave problem while only 500 cells were used in the flood wave problem.

Two different tests were performed. In the first test, gages 13, 15, 16, 18, A, B, C, and D were used (see Figure 7). In the second test, the eight numbered gages were used while the lettered gages were not used. The flow in the vicinity of the numbered gages is highly affected by wave shoaling, refraction, and diffraction processes, so the second test represents a more challenging problem for the method to solve.

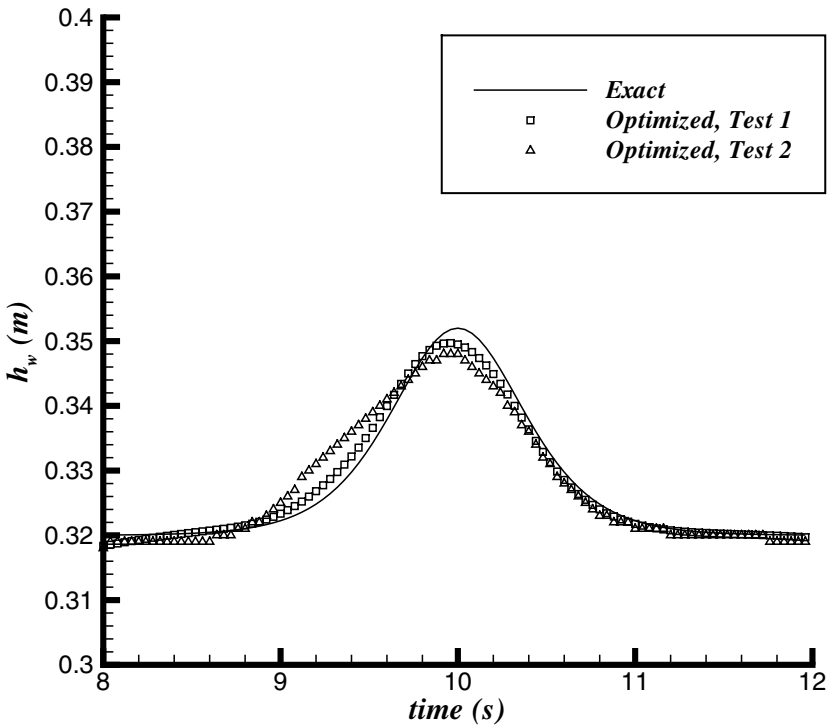

Figure 8. Optimized values of the solitary wave characteristics, $h_w(t)$, compared to the exact values.

In the first test, the objective function was initially $J = 6.5 \times 10^{-3}\,\mathrm{m^2\,s^{-1}}$ and it was reduced to $J = 9.6 \times 10^{-6}\,\mathrm{m^2\,s^{-1}}$ (0.15 per cent of the initial value) after 100 iterations. In the second test, the objective function was initially $J = 7.9 \times 10^{-3}\,\mathrm{m^2\,s^{-1}}$ and it was reduced to $J = 6.3 \times 10^{-5}\,\mathrm{m^2\,s^{-1}}$ (0.80 per cent of the initial value) after 100 iterations. The water level at the boundary $h_w(t)$ used to generate the gage data and the water level optimized in each test are shown Figure 8. The fact that the objective function was not reduced in the second problem as greatly as it was in the first is not surprising since the second problem involves much more complicated wave propagation phenomena. This result points to the importance of carefully selected gaging sites for the purpose of characterizing the deep sea properties of tsunamis.

CONCLUSIONS

The differential form of the adjoint shallow-water equations was solved in generalized two-dimensional coordinates by a fluctuation-splitting method that yields a high-resolution, monotone solution. The solution was obtained with one-step and two-step integration methods, both of which achieved solutions of equivalent accuracy with minimal numerical dissipation in a one-dimensional test problem with steady, uniform wave speeds. In addition, both schemes yielded much better results than the finite difference leap-frog method. However, the two-step

method was shown to be more accurate than the one-step method in problems with unsteady wave speeds, which is a common occurrence in open channel flow.

The two-step scheme was also tested in two-dimensions in the context of several parameter identification problems. Based upon the convergence characteristics observed during gradient-based optimization, the scheme was found to accurately propagate adjoint variable information in an irregular, two-dimensional domain with variable bathymetry and bottom friction, and even in the presence of nonlinear water waves. The resulting adjoint information allowed the inflow discharge in a river reach to be determined in real-time based on measurements of depth. In addition, the adjoint information allowed the far field characteristics of a long wave to be determined based on near field measurements of depth. In each test, an estimate of the parameter space was identified that reduced the objective function to less than 1 per cent of its original value. In addition, the adjoint numerical solution remained stable even in the presence of sharp fronts in the direct problem and the resulting sudden changes in the magnitude of the adjoint problem source term, $\partial r/\partial h$.

Both the shallow-water and adjoint shallow-water models are explicit and stable for Courant numbers less than one. Consequently, solutions of the direct and adjoint problems are easily obtained on desktop computers. A disadvantage of adjoint methods arises from the need to save the forward problem solution at each time level, thus using significant amounts of memory or file space. Using a grid containing 500 computational cells and marching 500 time steps, required approximately 11 MB of RAM. However, this problem is not unique to adjoint methods. For example, alternative parameter identification methods such as genetic algorithms also require substantial computer memory.

ACKNOWLEDGEMENTS

This research was made possible by a grant from the National Science Foundation (# CMS-9984579), whose support of the first author is gratefully acknowledged.

REFERENCES

1. Marchuk GI. *Adjoint Equations and Analysis of Complex Systems*. Kluwer, 1995.
2. Panchang VG, O'Brien JJ. On the determination of hydraulic model parameters using the adjoint state formulation. *Modeling Marine Systems*, vol. I, Davies AM (ed.). CRC Press, 1989; 5–18.
3. Das SK, Lardner RW. On the estimation of parameters of hydraulic models by assimilation of periodic tidal data. *Journal of Geophysical Research* 1991; **96**(C8):15 187–15 196.
4. Lardner RW. Optimal control of open boundary conditions for a numerical tidal model. *Computer Methods in Applied Mechanics and Engineering* 1993; **102**:367–387.
5. Liggett
JA, Chen L-C. Inverse transient analysis in pipe networks. *Journal of Hydraulic Engineering* 1994; **120**(4): 934–952.
6. Chertok DL, Lardner RW. Variational data assimilation for a nonlinear hydraulic model. *Applied Mathematical Modeling* 1996; **20**:675–682.
7. Katopodes ND, Piasecki M. Site and size optimization of contaminant sources in surface water systems. *Journal of Environmental Engineering* 1996; **122**:917–923.
8. Piasecki M, Katopodes ND. Control of contaminant releases in rivers. I: Adjoint sensitivity analysis. *Journal of Hydraulic Engineering* 1997; **123**:486–492.
9. Piasecki M, Katopodes ND. Control of contaminant releases in rivers. II: Optimal design. *Journal of Hydraulic Engineering* 1997; **123**:493–503.
10. Sanders BF, Katopodes ND. Control of canal flow by adjoint sensitivity method. *Journal of Irrigation and Drainage Engineering* 1999; **125**(5):287–297.
11. Alcrudo F, Garcia-Navarro P. A high-resolution Godunov-type scheme in finite volumes for the 2D shallow-water equations. *Int. Journal of Numerical Methods in Fluids* 1993; **16**:489–505.

12. Zhao DH, Shen HW, Tabios III GQ, Lai JS, Tan WY. Finite-volume two-dimensional unsteady-flow model for river basins. *Journal of Hydraulic Engineering* 1994; **120**:863–883.
13. Nujić M. Efficient implementation of non-oscillatory schemes for the computation of free-surface flows. *Journal of Hydraulic Research* 1995; **33**:101–111.
14. Ye J, McCorquodale JA. Depth-averaged hydrodynamic model in curvilinear collocated grid. *Journal of Hydraulic Engineering* 1997; **123**(5):380–388.
15. Bradford SF, Katopodes ND. Hydrodynamics of turbid underflows. Part I: Formulation and numerical analysis. *Journal of Hydraulic Engineering* 1999; **125**:1006–1015.
16. Hirsch C. *Numerical Computation of Internal and External Flows*, vol. 2. John Wiley & Sons: Chichester, 1990.
17. Sanders BF, Katopodes ND. Adjoint sensitivity analysis for shallow-water wave control. *Journal of Engineering Mechanics* 2000: **126**(9):909–297.
18. Sanders BF. Control of shallow-water flow using the adjoint sensitivity method. Ph.D Thesis, Department of Civil and Environmental Engineering, University of Michigan, 1997.
19. Roe PL. Approximate Riemann solvers, parameter vectors, and difference schemes. *Journal of Computational Physics* 1981; **43**:357–372.
20. LeVeque RJ. Wave propagation algorithms for multidimensional hyperbolic systems. *Journal of Computational Physics* 1997; **131**:327–353.
21. Van Albada GD, Van Leer B, Roberts WW. A comparative study of computational methods in cosmic gas dynamics. *Astronomy and Astrophysics* 1982; **108**:76–84.
22. Bradford SF, Sanders BF. Finite volume model for shallow-water flooding and drying of arbitrary topography. *Journal of Hydraulic Engineering*, to appear.
23. Van Leer B. Towards the ultimate conservative difference scheme. V. A second order sequel to Godunov's method. *Journal of Computational Physics* 1979; **32**:101–136.
24. Glaister P. Approximate Riemann solution of the two-dimensional shallow-water equations. *Journal of Engineering Mathematics* 1980; **24**:45–53.
25. Sweby PK. High resolution schemes using flux limiters for hyperbolic conservation laws. *SIAM Journal of Numerical Analysis* 1984; **21**:995–1011.
26. Shanno DF, Phua KH. Remark on Algorithm 500, a variable metric method for unconstrained minimization. *ACM Transactions on Mathematical Software* 1980; **6**:618–622.
27. Press WH, Teukolsky SA, Vetterling WT, Flannery BP. *Numerical Recipes in FORTRAN*. Cambridge University Press: Cambridge, 1992.
28. Briggs MJ, Synolakis CE, Harkins GS, Green DR. Laboratory experiments of tsunami runup on a circular island. *Pure and Applied Geophysics* 1995; **144**:569–593.
29. Liu PLF, Cho Y, Briggs MJ, Kanoglu U, Synolakis CE. Runup of solitary waves on a circular island. *Journal of Fluid Mechanics* 1995; **302**:259–285.
30. Titov VV, Synolakis CE. Numerical modeling of tidal wave runup. *Journal of Waterway*, *Port*, *Coastal*, *and Ocean Engineering* 1998; **124**:157–171.

